Biological and Medical Applications of Materials and Interfaces

DNA Functionalized Porous Fe3O4 Nanoparticles for the Construction of Self-Powered miRNA Biosensor with Target Recycling Amplification

Tian Zhang, Hua Chai, Fanyu Meng, Zhenzhen Guo, Yu Jiang, and Peng Miao

ACS Appl. Mater. Interfaces, **Just Accepted Manuscript** • DOI: 10.1021/acsami.8b15419 • Publication Date (Web): 10 Oct 2018

DNA Functionalized Porous Fe_3O_4 Nanoparticles for the Construction of Self-Powered miRNA Biosensor with Target Recycling Amplification

Tian Zhang,[†,‡] Hua Chai,[†,‡] Fanyu Meng,[†,‡] Zhenzhen Guo,[‡] Yu Jiang,[*,§] and Peng Miao[*,†,‡]

[†] University of Science and Technology of China, Hefei 230026, People's Republic of China

[‡] Suzhou Institute of Biomedical Engineering and Technology, Chinese Academy of Sciences, Suzhou 215163, People's Republic of China

[§] Department of Orthopedics, Nanjing Medical University Affiliated Wuxi Second Hospital, Wuxi 214000, People's Republic of China

KEYWORDS: biofuel cells; electrochemical biosensor; miRNA; porous Fe_3O_4 nanoparticles; duplex specific nuclease.

ABSTRACT: Herein, we have developed an ultrasensitive self-powered biosensor for miRNA assay based on biofuel cells (BFCs). The system is composed of indium tin oxide cathode and graphene oxide/gold nanoparticles/glucose oxidase anode. Redox probe of $[Fe(CN)_6]^{3-}$ is entrapped inside porous Fe_3O_4 nanoparticles by DNA. However, in the presence of target miRNA, hybridization reaction occurs between miRNA and DNA, which initiates the release of $[Fe(CN)_6]^{3-}$. Moreover, duplex specific nuclease is further employed to trigger target recycling amplification. As a result, much more redox probes are released and the open circuit voltage is significantly increased. A "signal-on" self-powered biosensor for miRNA quantification is thus developed. The detection range is from 10 aM to 10 fM; meanwhile, the limit of detection is as low as 1.4 aM, which is superior to most reported methods. Therefore, the proposed biosensor is expected to be a powerful point-of-care tool for miRNA diagnostics, which may have wide applications in the future.

INTRODUCTION

miRNAs are a group of short non-coding small RNAs, which function as important gene regulators for various cellular processes. More and more researches have revealed that miRNA expression is closely related with many types of diseases such as neurodegeneration,[1] diabetes,[2] virus caused disorders,[3] and cancers.[4] miRNAs are becoming novel biomarkers for disease diagnosis with great clinical values.[5-8] However, most traditional techniques like quantitative reverse transcription polymerase chain reaction (qRT-PCR),[9] sequencing,[10] and nanostring technology[11] are too complicated and not suitable for point-of-care testing applications. Up to now, miRNA biosensors have been paid more and more attention and various biosensors have been fabricated.[12-15] For example, Congur et al. modified pencil graphite electrodes with graphene oxide (GO) and constructed an impedimetric sensor to monitor miR-34a.[16] Lv et al. fabricated a facile resonance light scattering (RLS) sensor to probe miR-122 using novel CdTe quantum dots.[17] Lee et al. synthesized self-assembling magnetic fluorescence nanoparticles (NPs) and developed a novel magnetic resonance imaging (MRI) method to monitor intracellular miR-124a.[18] Liu et al. invented a flowerlike nanovector for fluorescent detection of miR-21 with catalytic hairpin assembly.[19] Cheng et al. devised a target-triggered isothermal amplification strategy for miR-21 assay combining polymerase-nicking enzyme cascade and DNAzyme.[20] Koo et al. reported an amplification-free strategy for miRNA detection based on increased affinity interaction between polyadenylated miRNA and bare gold electrode.[21-22] However, due to the unique characteristics of miRNA (e.g., small size, low abundance, high homology), it still remains a challenge to develop novel methods for ultrasensitive miRNA profiling for practical use.

Biofuel cells (BFCs) are a type of fuel cells which use enzymes or bacteria to produce sustainable energy under mild conditions for further applications.[23-24] BFCs have now received tremendous attention.[25-26] Generally, a BFC is an energy conversion device which functions with simple electrochemical principles and catalysts.[27] Recent years have witnessed a great progress in the aspects of BFC-based self-powered biosensors, which have unique properties such as low cost, small size, simple construction procedure, and so on.[28-29] Most importantly, due to the self-charging power system of BFC, there is no need for external power sources.[30] Therefore, BFC-based biosensors greatly satisfy the requirements of practical point-of-care testing applications, which are distinct from traditional biosensors.

In this contribution, we have developed a novel self-powered biosensor for the detection of miRNA. Different nanomaterials have been applied to construct cathode and anode, including gold nanoparticles (AuNPs), magnetic NPs and GO. Porous magnetic materials are introduced in the BFC-based biosensing system for the first time. They are facilely synthesized with appropriate pore size to load electrochemical species, which are sealed by complementary DNA (cDNA) responding to target miRNA. The applied Fe_3O_4 NPs are not only uniform but also possess magnetic property for a convenient separation purpose, which show significant superiority over other porous materials like widely used mesoporous silica NPs. In addition, current BFC-based biosensors or electrochemical biosensors always involve the immobilization process of recognition probes or signal probes on the electrodes, which may require complicated experimental steps and lead to unsatisfactory reproducibility.[31-32] In this work, the fabricated porous Fe_3O_4 NPs integrate the recognition probe and signal probe, which benefit the homogeneous electrochemical assay of targets without any immobilization procedures. Furthermore, duplex specific nuclease (DSN)-catalyzed reaction is designed and employed for

target recycling amplification. Ultrahigh sensitivity for miRNA assay is thus promised. This proposed method integrates merits of BFC-self powered system, porous magnetic NPs, and enzyme-catalyzed amplification, which holds great potential as a powerful tool for miRNA diagnostics.

EXPERIMENTAL SECTION

Materials and Instruments. Iron (III) chloride hexahydrate ($FeCl_3 \cdot 6H_2O$), urea, polyacrylamide, poly(diallyldimethylammonium chloride) (PDDA), diethypyrocarbonate (DEPC), 1-ethyl-3-[3-dimethylaminopropyl]carbodiimide hydrochloride (EDC), *N*-hydroxyosuccinimide (NHS), and glucose oxidase from *Aspergillus niger* (100 – 250 units mg^{-1}) were purchased from Sigma (USA). Chloroauric acid ($HAuCl_4$) and trisodium citrate were purchased from Shanghai Jiushan Chemicals Co., Ltd. (Shanghai, China). DSN was supplied by Genomax Technologies Pte Ltd. (Singapore). GO was obtained from Nanjing XFNANO Materials Tech Co., Ltd (Nanjing, China). Other reagents were of analytical grade and used without further treatment. Quant One Step qRT-PCR Kit was purchased from Tiangen Biotech Co., Ltd. (Beijing, China). Magnetic glassy carbon electrode was purchased from Tianjin Incole Union Technology Co., Ltd. (Tianjin, China). All oligonucleotides were obtained from Takara Biotechnology Co., Ltd. (Dalian, China). The sequences of DNA and RNA were shown in Table S1. Double-distilled water was purified with a Millipore system under 18 MΩ cm resistivity, which was treated with DEPC (0.1%) before use.

Electrochemical experiments were carried out on a CHI 660D electrochemical workstation (CH instruments, China). A three-electrode system was applied, which included an Ag/AgCl reference electrode, a platinum wire counter electrode and the fabricated anode or cathode

working electrode. Cyclic voltammetry (CV) and electrochemical impedance spectroscopy (EIS) experiments were conducted in 5 mM $[Fe(CN)_6]^{3-/4-}$ with 1 M KNO_3. The scan range was from +0.6 to -0.2 V and the scan rate of CV was 50 mV s^{-1}. The frequency range of EIS was from 0.1 to 100000 Hz. The open circuit voltage E^{OCV} of BFC was measured by connecting the anode and the cathode placed in the electrolytic cell. To demonstrate successful DNA modification, chronocoulometry (CC) is conducted in 10 mM Tris–HCl with 50 μM $[Ru(NH_3)_6]^{3+}$ (pH 7.4) with the working electrode of a magnetic glassy carbon electrode. Agrose gel electrophoresis was photographed under UV light by Gel Doc™ XR+ System (Bio-Rad, USA). qRT-PCR experiments were performed on an ABI 7500 Real-Time PCR System (ABI Life Technologies, USA). Transmission electron microscopic (TEM) images were acquired from a FEI Tecnai G20 transmission electron microscopy (FEI, USA). Magnetization curve was recorded by a vibrating sample magnetometer (Toei Industry Co., Ltd.). N_2 adsorption-desorption isotherm was characterized by a Micromeritics TriStar 3020 analyser (Micromeritics Instrument Corporation, USA). Zeta potential distribution was recorded by a Zetasizer (Malvern Instruments, Zetasizer Nano ZS90, UK).

Synthesis of PDDA-Capped Porous Fe_3O_4 NPs. Pristine porous Fe_3O_4 NPs were synthesized by means of a hydrothermal method according to a previous report with slight modifications.[33] Briefly, 0.5 g of ferric chloride, 1.5 g of sodium citrate dihydrate and 0.5 g of urea were dissolved in 40 mL of distilled water and the solution was stirred for 10 min. Next, 0.5 g of polyacrylamide dissolved in 40 mL of distilled water was added slowly with vigorous stirring. The mixture was then transferred into a 100 mL Teflon-lined autoclave and heated to 200°C for 12 h. Subsequently, the product was collected by magnetic separation and washed with absolute distilled water and ethanol for three times. The synthesized pristine NPs were dried

at 60 °C. After that, 10 mg of as-synthesized porous Fe_3O_4 NPs was added into 5 mL of PDDA solution (4.0 mg mL^{-1}, 0.05 M NaCl), which was then ultrasonicated for 1 h, generating a homogeneous suspension of positively charged NPs. Finally, the product was magnetically separated, washed, and dried.

$[Fe(CN)_6]^{3-}$ Loading and DNA Functionalization. 4 mg of PDDA-capped Fe_3O_4 NPs was dissolved into 1 mL of $[Fe(CN)_6]^{3-}$ solution with the concentration of 80 mM, which was then gently shaken at room temperature for 8 h. During this period, $[Fe(CN)_6]^{3-}$ entered the pores of the porous Fe_3O_4 NPs through diffusion process. Afterward, 1 μL of cDNA (10 μM) was added to the above solution. The mixture was gently shaken again at room temperature for 8 h. Subsequently, the nanocomposites was magnetically separated, washed, and resuspended in 1 mL of Tris-HCl buffer (pH 7.4) containing 0.1 M NaCl.

Preparation of GO/AuNPs/Glucose Oxidase Anode. AuNPs were synthesized by the citrate reduction of $HAuCl_4$ according to a previous report.[34] 10 mg of GO was added into 5 mL of PDDA solution (4.0 mg mL^{-1}, 0.05 M NaCl), which was then ultrasonicated for 1 h to form a homogeneous suspension of positively charged GO. After purified by centrifugation, GO was blended with 1 mL of AuNPs and the mixture was gently shaken for 8 h. The formed GO/AuNPs composites were also purified by centrifugation. Next, 100 μL of GO/AuNPs (1 mg mL^{-1}) was casted on the surface of indium tin oxide (ITO) substrate electrode at 37°C for 2 h. Then, the electrode was treated with EDC (200 mM) and NHS (50 mM) for 30 min in order to activate carboxyl groups. After careful rinsing, the electrode was incubated with 100 μL of glucose oxidase with the concentration of 10 mg mL^{-1} at 4°C for 16 h. Finally, the electrode was rinsed by pure water and then stored in phosphate buffer saline (pH 7.4) until use.

Electrochemical Measurement. A novel BFC was fabricated based on the modified anode and cathode with the electrolyte of Tris-HCl (100 mM, 5 mM glucose, pH 7.4). In the absence of miRNA, 40 μL of cDNA functionalized nanocomposites was spiked into 5 mL of supporting electrolyte. The measured open circuit voltage of BFC was defined as E_0^{OCV}. Next, 5 μL of miRNA sample with different concentrations, 40 μL of cDNA functionalized nanocomposites, and 5 μL of Tris-HCl (100 mM, 0.5 U DSN, 50 mM $MgCl_2$, 10 mM DTT, pH 8.0) were mixed and incubated at 50 °C for 2 h. Afterward, the solution was added to 5 mL of supporting electrolyte for the measurement of E^{OCV}.

RESULTS AND DISCUSSION

Sensing Principle. Scheme 1 illustrates detailed principle of the sensing strategy. The BFC-based self-powered biosensor is consisted of nanomaterials modified cathode and anode. Generally, anode is ITO electrode modified with GO/AuNPs/glucose oxidase. Cathode is associated with DNA functionalized Fe_3O_4 NPs. The porous Fe_3O_4 NPs are firstly capped with positive PDDA, which then encapsulate redox probes of $[Fe(CN)_6]^{3-}$ through the pores. Next, cDNA is employed to block the pores by electrostatic interaction. Since $[Fe(CN)_6]^{3-}$ is effectively encapsulated in the NPs, a low open circuit voltage (E^{OCV}) is obtained. However, in the presence of miRNA, cDNA hybridizes with miRNA to form rigid DNA/RNA duplex and the pore is opened. In addition, DSN is applied which specially digest DNA strand in DNA/RNA duplex (inset in Figure S1); meanwhile, miRNA is released to hybridize additional cDNA around NPs for next cycles of digestion. Finally, trace miRNA can be used to open multiple pores for controlled release of $[Fe(CN)_6]^{3-}$. The Zeta potentials during each steps are recorded, which confirm the hypothesis about construction of DNA functionalized NPs and DSN-catalyzed digestion (Figure S1). After capped with PDDA, the NPs show a highly positive Zeta potential

benefited from the adsorption of the positively charged layer. A reversal is observed after further functionalization of DNA with negative phosphate backbone. In the absence of target miRNA, DSN cannot be used to digest the cDNA, thus, the Zeta potential barely changes. However, the coexistence of miRNA and DSN initiate cycling digestion of cDNA. As a result, significantly reduced Zeta potential is achieved. On the other hand, with effective glucose oxidation on the anode, electrons produced by the anode could be transferred to cathode, resulting in the reduction of $[Fe(CN)_6]^{3-}$. Therefore, E^{OCV} is increased remarkably, which could be used to indicate initial concentration of target miRNA.

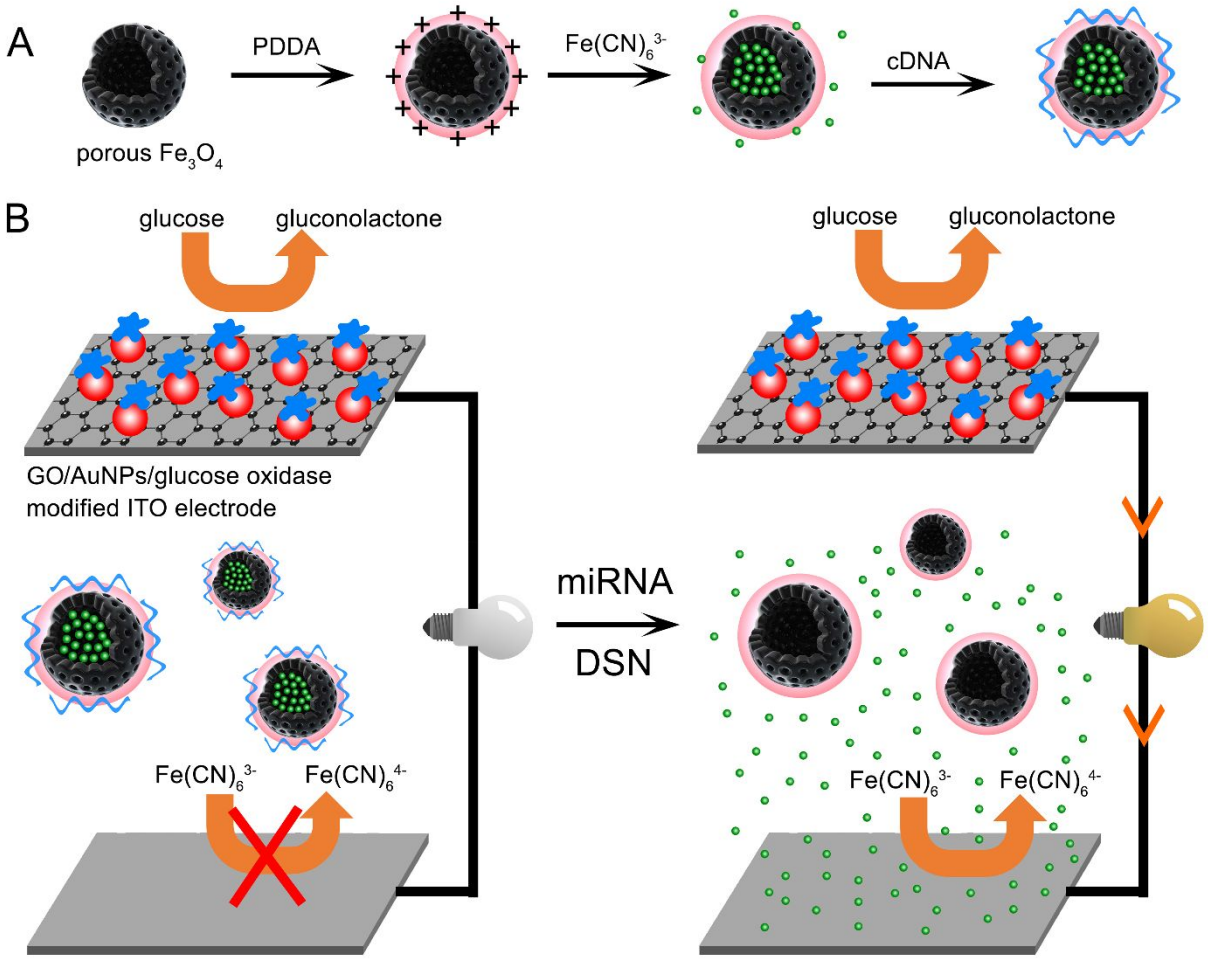

Scheme 1. (A) Preparation process of DNA functionalized porous Fe_3O_4 NPs. (B) Schematic illustration of the working principle of the self-powered biosensor with DSN-assisted amplification.

Characterization of BFC Cathode and Anode. Figure 1A is a typical TEM image of the synthesized bare Fe_3O_4 NPs. Spherical nanoparticles are observed with an average diameter of 250 nm, which have light and dark regions. The contrast suggests hollow structures of the spheres. The magnetic property of the NPs are important, which facilitates multiple modification and separation steps. Therefore, magnetization curve is recorded which reveals excellent paramagnetic property as well as high separation efficiency (Figure 1B). In order to evaluate porosity of the NPs, N_2 adsorption-desorption isotherm and pore size distribution curve are depicted (Figure 1C and D). Well-defined pore size is about 6.5 nm, thus efficient loading of redox probes is guaranteed. To demonstrate the successful modification of DNA onto the surface of NPs, PDDA modified Fe_3O_4 NPs before and after DNA treatment are immobilized on the surface of the magnetic glassy carbon electrode for CC characterizations. The curve corresponding to DNA functionalized Fe_3O_4 NPs is much higher than that of pristine PDDA modified NPs. This is due to the higher charge density of $[Ru(NH_3)_6]^{3+}$ molecules which are specially absorbed on the phosphate backbone of the modified DNA (Figure S2).

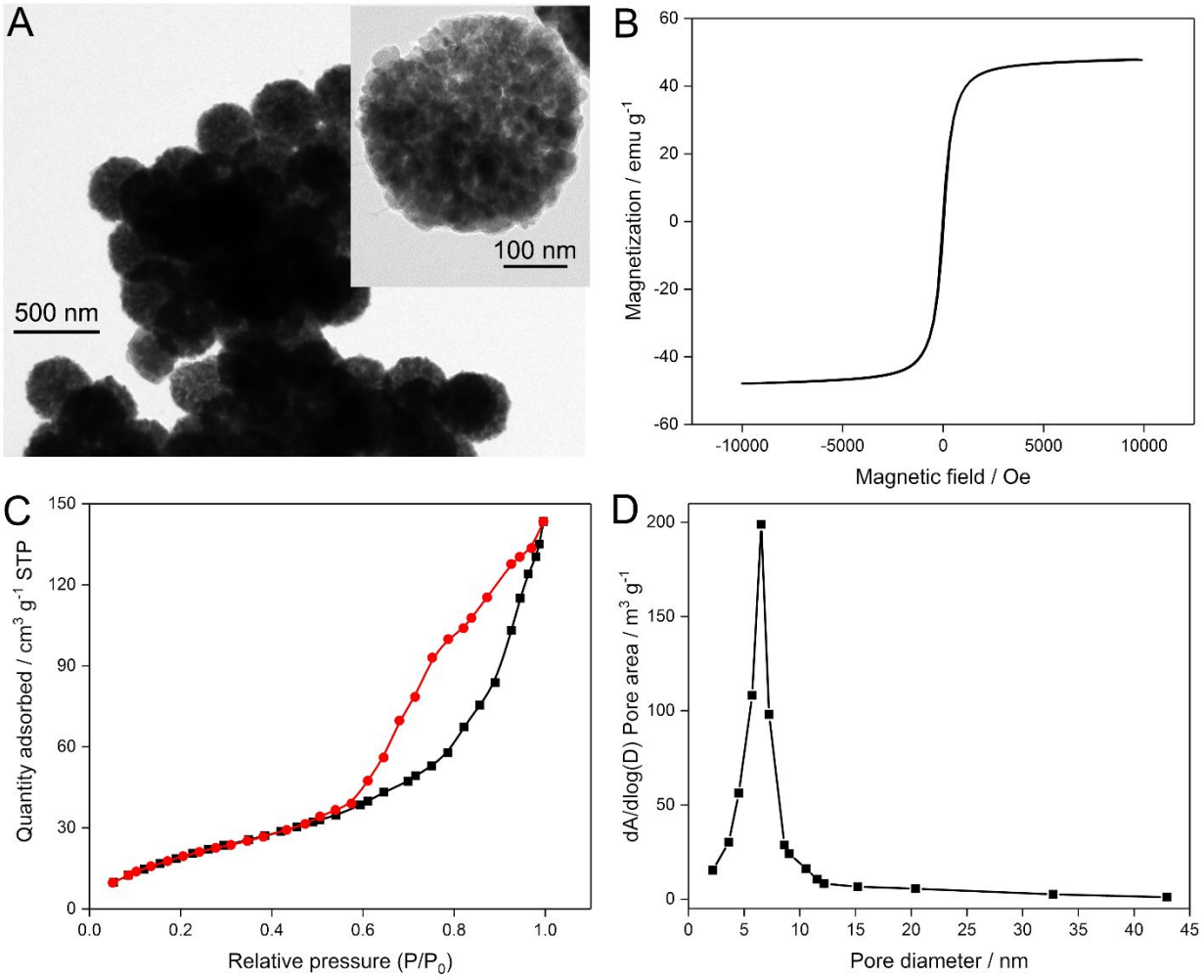

Figure 1. (A) TEM images of the porous Fe_3O_4 NPs. (B) Magnetization curve of the porous Fe_3O_4 NPs. (C) N_2 adsorption-desorption isotherms of the porous Fe_3O_4 NPs. (D) Pore size distribution plot.

BFC anode is an important component for the generation of electrons. To achieve efficient immobilization of glucose oxidase, GO/AuNPs are used as the matrix, which have excellent biocompatibility and good electrical conductivity. The morphologies of GO and GO/AuNPs are also characterized by TEM (Figure 2A and B). AuNPs are well dispersed with the diameter of 13 nm and decorated on the surface of GO. The nanocomposites are suitable for subsequent

immobilization of multiple glucose oxidase. Each modification step of anode is studied by EIS. In a typical impedance spectrum, semicircle portion is related to the electron transfer limited process. As shown in Figure 2C, after the modification of GO/AuNPs, the semicircle decreases, which is due to the excellent electrical conductivity of the matrix. However, after further loading of glucose oxidase, a much larger semicircle is observed which demonstrates the large impedance caused by the modified glucose oxidase. CV is then applied to investigate the cathodic signals. As shown in Figure 2D, in the absence of miRNA, due to the block of the redox probes, a pair of small peaks are observed (curve a). After the employment of miRNA, which hybridizes with cDNA, the released of cDNA leads to the leakage of redox probes. Therefore, the peak intensities increase (curve b). Moreover, after further employment of DSN digestion, which triggers target recycling amplification, the peak intensities become even larger with more leaked redox probes (curve c). These results have successfully demonstrated the feasibility of the BFC-based self-powered biosensor.

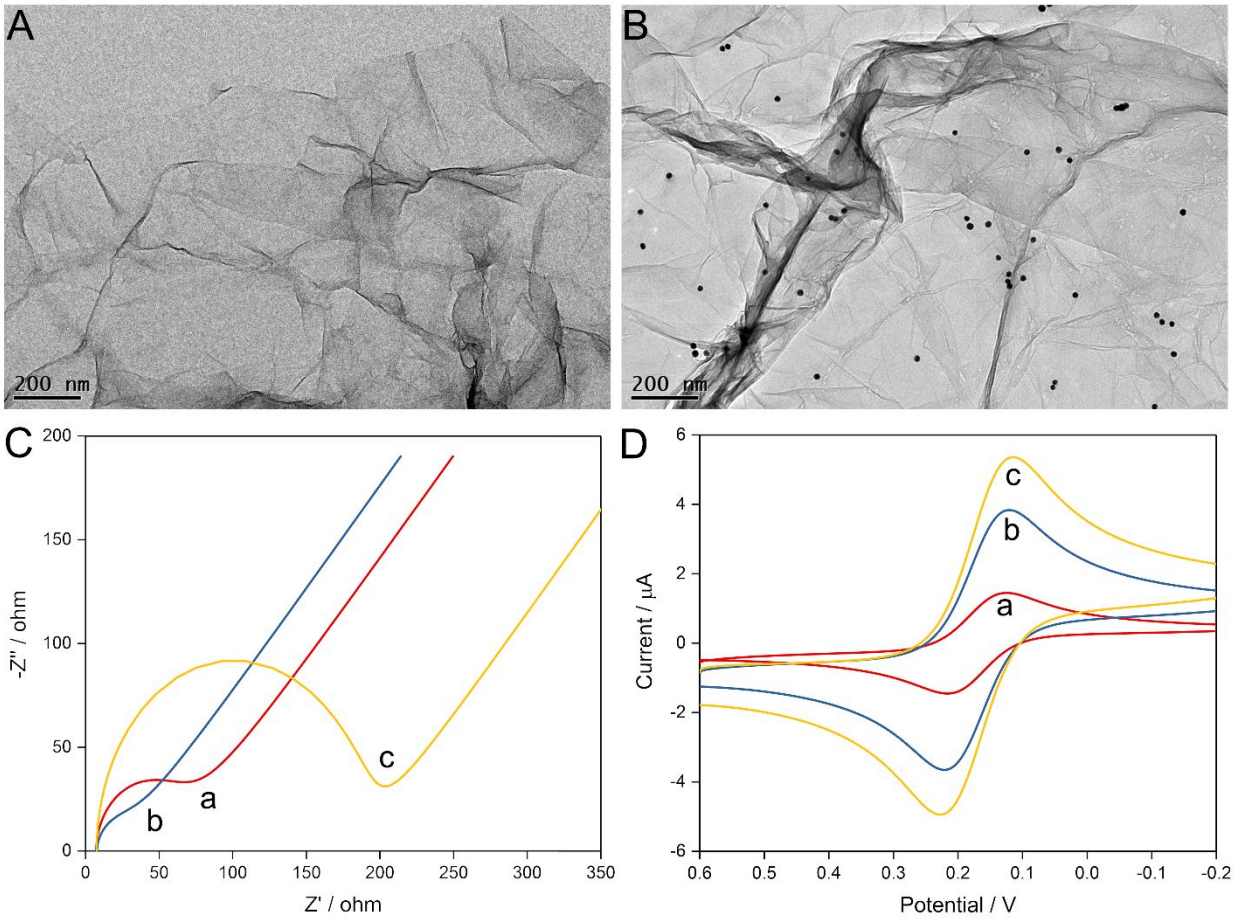

Figure 2. TEM images of (A) GO, (B) GO/AuNPs. (C) Nyquist plots corresponding to (a) bare ITO electrode, (b) GO/AuNPs modified ITO electrode, and (c) GO/AuNPs/glucose oxidase modified ITO electrode. (D) Cyclic voltammograms of $[Fe(CN)_6]^{3-}$ at the cathode in the (a) absence and presence of miRNA (b) without and (c) with DSN-assisted amplification.

Optimization Experiments. To ensure high performance of this self-powered biosensing system, a series of experimental conditions are optimized using the technique of cyclic voltammetry. Typically, the signal intensity relies on the amount of $[Fe(CN)_6]^{3-}$ loaded inside Fe_3O_4 NPs. The loading density is dependent on the concentration of environmental $[Fe(CN)_6]^{3-}$ during the encapsulating step, which diffuses into the pores of the NPs. With the

increase of the environmental $[Fe(CN)_6]^{3-}$ level, more redox probes are supposed to be encapsulated with a dynamic equilibrium. We have tested different levels of environmental $[Fe(CN)_6]^{3-}$ and CV peak currents are recorded for comparison. An optimized concentration of 80 mM is chosen for subsequent experiments (Figure S3A). Similarly, we have studied the effect of Fe_3O_4 NPs concentration. The CV peak current increases with more Fe_3O_4 NPs (Figure S3B). The peak reaches a plateau when the concentrations is up to 4 mg mL^{-1}, which is then used as the optimized value. The effect of cDNA concentration used to block the pores of Fe_3O_4 NPs is also investigated. Initially, less cDNA cannot completely block the release of $[Fe(CN)_6]^{3-}$ from Fe_3O_4 NPs. The final amount of the redox probes inside the NPs is limited after magnetic separation. With the increase of cDNA, more redox probes are sealed, which are available for subsequent electrochemical biosensing. Consequently, the peak current increases (Figure S3C). After the cDNA concentration is increased to 10 nM, the peak intensity reaches the saturation. Therefore, 10 nM is chosen as the optimized concentration. Since the hybridization reaction, DSN-catalyzed digestion and redox probe release are implemented simultaneously, we have studied the effect of reaction time on the recorded electrochemical signal. Maximum CV peak current is achieved after 120 min, the time of which is applied in the following experiments (Figure S3D).

Quantitative Analysis of miRNA. Under optimized experimental conditions, quantitative detection of miRNA is investigated by comparing the increased values of the open circuit voltages of BFC biosensor after miRNA-triggered recycling release of $[Fe(CN)_6]^{3-}$. As shown in Figure 3A, without miRNA, the E^{OCV} is as low as 0.405 V, which is due to the fact that nearly no $[Fe(CN)_6]^{3-}$ exists as the electron acceptor. However, in the presence of miRNA, DNA/RNA

duplex forms by cDNA and miRNA. $[Fe(CN)_6]^{3-}$ can then be released from the opened pores and increased E^{OCV} is achieved, which is closely related to the concentration of introduced miRNA. In addition, we have also recorded E^{OCV} values when DSN is employed to initiate target recycling amplification (Figure 3B). Theoretically, less miRNA is required to liberate equal amount of cDNA assisted by DSN. We have compared the relationships between miRNA concentration and ΔE^{OCV} in the absence and presence of DSN in Figure 3C, the results of which have confirmed our hypothesis. With DSN digestion, a wide linear range is obtained from 10^{-17} to 10^{-14} M with the following equation:

$$y = 0.6937 + 0.0393 \log x \ (R^2 = 0.9954, n = 3)$$

in which, y stands for ΔE^{OCV}, x is the logarithmic miRNA concentration (Figure 3D). The limit of detection (LOD) as low as 1.4 aM is calculated (signal-to-noise ratio of 3). The ultrahigh sensitivity is attributed to two reasons. First, the porous Fe_3O_4 nanoparticles provide a huge physical 3D space for the loading of redox probe of $[Fe(CN)_6]^{3-}$. Second, DSN is able to digest DNA from the hybridized DNA/RNA duplex formed by target miRNA and cDNA. The recycling digestion reaction consumes a large number of cDNA, and the pores on Fe_3O_4 nanoparticles can be opened to release $[Fe(CN)_6]^{3-}$. We have compared the analytical performances with recently developed miRNA biosensors with different detection techniques in Table 1. Most of current analytical methods involve single or no amplification process, while the proposed method is enhanced by DSN-catalyzed digestion cycle and porous Fe_3O_4 NPs-aided signal enrichment. Inspiringly, LOD of our method is the lowest, demonstrating the ultrahigh sensitivity of this method. The dynamic concentration range of 3 orders of magnitude is quite wide. To study the stability of this BFC-based self-powered biosensor, the cathode and anode are prepared and then stored at 4°C. After 1 month, the biosensing system is constructed. The

electrochemical responses are recorded and compared with freshly prepared cathode and anode. Over 94% of original signal intensity is obtained, which demonstrates the high stability of the developed biosensor.

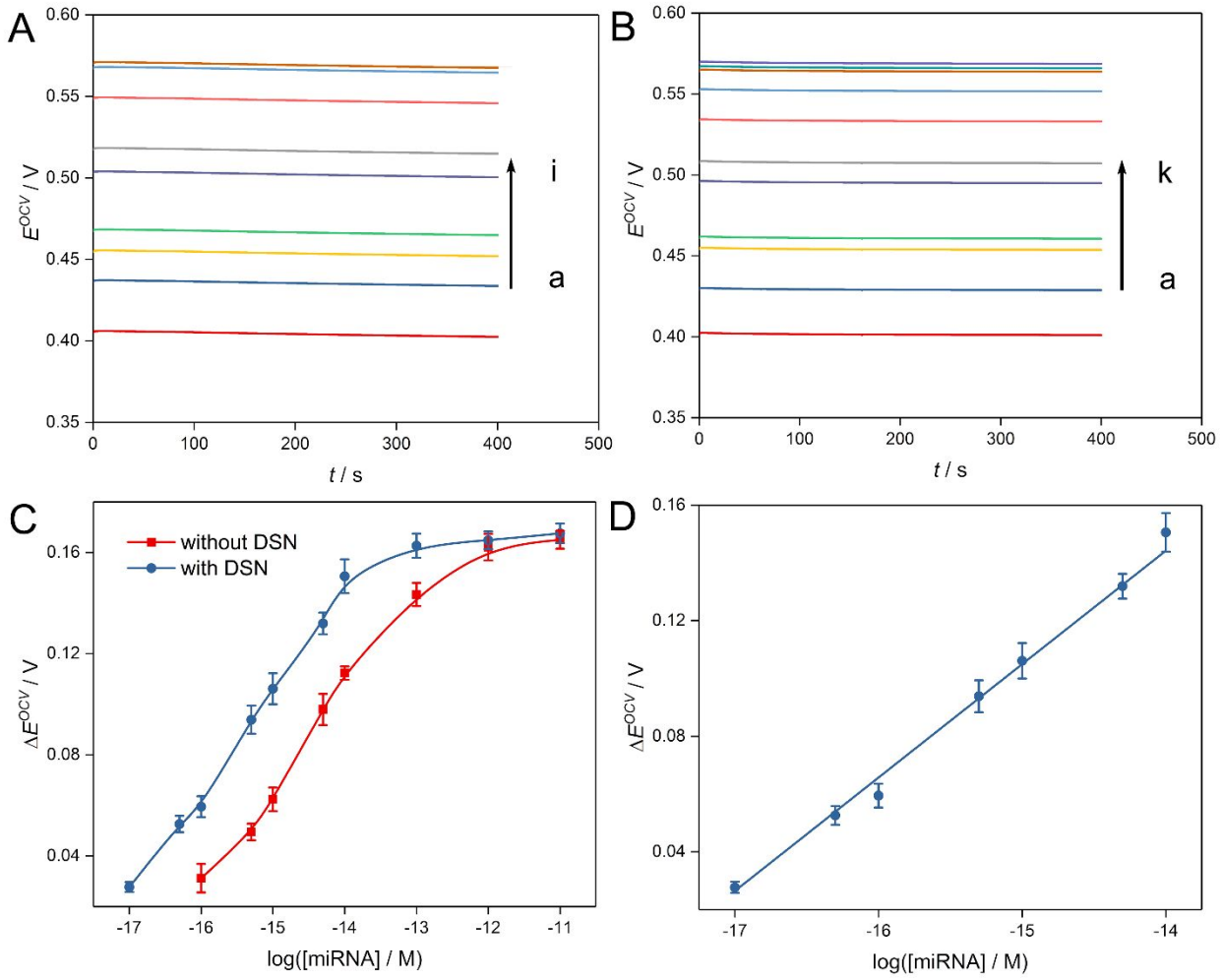

Figure 3. (A) E^{OCV} of the self-powered biosensor for the detection of miRNA without DSN: (a to i), 0, 10^{-16}, 5×10^{-15}, 10^{-15}, 5×10^{-14}, 10^{-14}, 10^{-13}, 10^{-12}, 10^{-11} M. (B) E^{OCV} of the self-powered biosensor for the detection of miRNA with DSN-assisted amplification: (a to k), 0, 10^{-17}, 5×10^{-16}, 10^{-16}, 5×10^{-15}, 10^{-15}, 5×10^{-14}, 10^{-14}, 10^{-13}, 10^{-12}, 10^{-11} M. (C) The calibration curves of increased E^{OCV} values versus logarithmic miRNA concentrations in the absence and presence of DSN-

assisted amplification. (D) shows the curve reflecting the linear relationship between ΔE^{OCV} and logarithmic miRNA concentration in the presence of DSN. Error bars represent standard deviation of three independent measurements.

Table 1. Comparison of analytical performances of the proposed method with recently developed miRNA biosensors.

Technique	Strategy	Linear range (M)	LOD (M)	Ref
Fluorescence	DNA circuit-assisted GO enhanced system	0 to 1.6×10^{-8}	4.7×10^{-11}	35
Fluorescence	two stages DSN-assisted target recycling	10^{-12} to 10^{-5}	1.03×10^{-12}	36
CC	gold-loaded nanoporous superparamagnetic nanocubes	10^{-13} to 10^{-6}	10^{-13}	37
Gel assay	catalytic hairpin assembly	10^{-13} to 10^{-9}	10^{-14}	38
colorimetry	pH-responsive isothermal amplified system	2×10^{-14} to 2×10^{-8}	9.3×10^{-15}	39
electrophoresis	separation-assisted double cycling signal amplification	2×10^{-14} to 2×10^{-11}	8×10^{-15}	40
CC	Au-loaded nanoporous ferric oxide nanocubes	10^{-16} to 10^{-9}	10^{-16}	41
SPR	Au@Ag nanorods etching	5×10^{-17} to 10^{-11}	5×10^{-17}	42
PEC	target recycling by T7 exonuclease	8×10^{-17} to $\times10^{-11}$	2.7×10^{-17}	43
CC	bridge DNA−AuNPs and DSN	10^{-17} to 10^{-11}	6.8×10^{-18}	44

SWV	cascade strand displacement polymerization	10^{-17} to 5×10^{-15}	3.2×10^{-18}	45
BFC	DNA functionalized porous Fe_3O_4 NPs and DSN	10^{-17} to 10^{-14}	1.4×10^{-18}	this method

SPR: surface plasmon resonance, PEC: photoelectrochemistry; CC: chronocoulometry; SWV: square wave voltammetry;

Reproducibility and Selectivity Investigation. Reproducibility of this method is studied by repeated detection of miRNA using different sets of DNA functionalized porous Fe_3O_4 NPs. Since the synthesis of Fe_3O_4 NPs is a one-pot process, and the magnetic separation is quite efficient, the properties of the products are quite consistent between different sets, which are superior to other nanomaterials with complicated preparation processes. Therefore, the finally obtained open circuit voltages are nearly the same, which guarantees excellent reproducibility (Figure S4). In addition, we have employed random DNA (rDNA) to block the porous Fe_3O_4 NPs. Since its sequence is not complementary with target miRNA. Hybridization reaction does not occur and the $[Fe(CN)_6]^{3-}$ is not released since rDNA still seals the pores. Therefore, the open circuit voltages barely change even with high concentrations of miRNA, which are distinctive from the results of cDNA functionalized porous NPs (Figure 4A). To check the specificity of this miRNA biosensor, five interfering homologous miRNAs are challenged. Due to the small size of miRNAs, the interfering miRNAs with single or double mismatched sites cannot completely hybridize with cDNA, which are different from long RNA strands. On the other hand, DSN is a type of nuclease which specially hydrolyzes DNA strand in the DNA/RNA heteroduplex. Therefore, single-stranded cDNA cannot be digested unless target

miRNA-assisted complete hybridization. As shown in Figure 4B, negligible ΔE^{OCV} values are detected using interfering miRNAs in contrast to the high response in the presence of target miRNA. The results have indicated excellent specificity and selectivity of this biosensor.

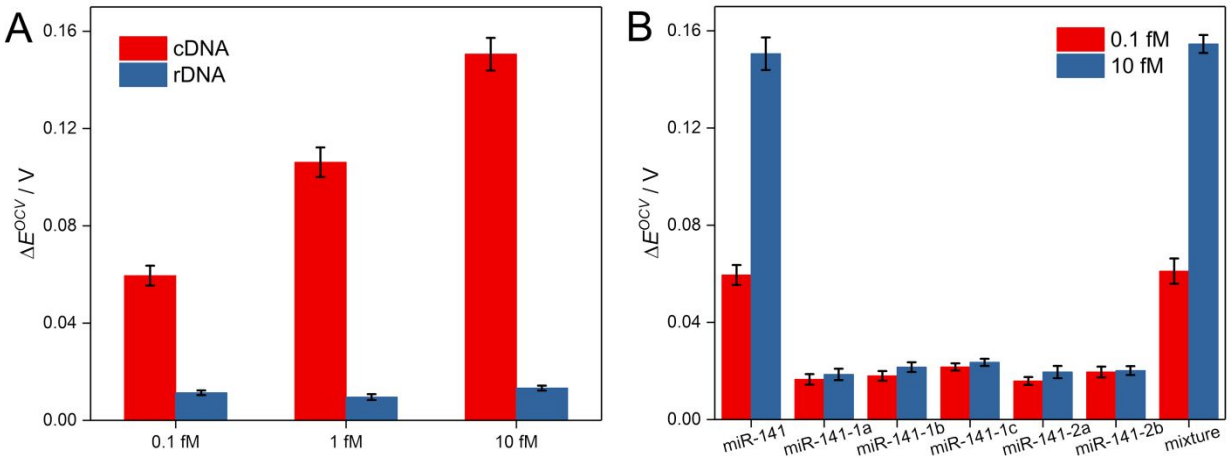

Figure 4. (A) ΔE^{OCV} of the self-powered biosensor constructed with cDNA and rDNA for the detection of different amount of target miRNA. (B) Selectivity investigation of the self-powered biosensor for the analysis of different miRNAs.

Verification of Practical Utility. After establishing the sensitivity and specificity, we have performed clinical validation of this biosensor by analyzing miRNA levels in human serum samples, which are firstly diluted for 10 times with PBS. Standard addition method is applied. Detection of miRNA in serum samples can be achieved without any pretreatments like separation or enrichment. As shown in Table 2, the obtained results are in good accordance with those of standard qRT-PCR Kit, demonstrating the effectiveness of this miRNA assay. Recoveries are from 98.60% to 104.00% and Relative errors are less than 4%. These results clearly suggest that the proposed self-powered biosensor has great potential applications for clinical miRNA diagnostics.

Table 2. Measurements of miR-141 in human serum samples.

Sample	Added (fM)	Determined (fM)	qRT-PCR results (fM)	Recovery (%)	Relative error (%)
1	1.00	1.01	0.98	101.00	3.06
	10.00	10.40	10.19	104.00	2.06
2	1.00	0.97	0.99	97.00	2.02
	10.00	9.86	10.08	98.60	2.18

CONCLUSIONS

In summary, we have developed a novel BFC-based biosensor for ultrasensitive detection of miRNA coupling DNA functionalized porous Fe_3O_4 nanoparticles and DSN-mediated recycling amplification. The porous Fe_3O_4 nanoparticles not only assist the loading of numerous redox probes, but also facilitate the preparation of functionalized nanomaterials with magnetic separation. Target miRNA triggers cDNA liberation and the subsequent release of $[Fe(CN)_6]^{3-}$ enables self-powered electrochemical biosensing. In addition, DSN-catalyzed reactions significantly enhance the signals, thus ultrahigh sensitivity is achieved with a LOD as low as 1.4 aM. Excellent selectivity is shown to distinguish similar miRNAs. The proposed biosensor is also much easy to be extended to detect other targets of interest in practical applications.

ASSOCIATED CONTENT

Supporting Information

The Supporting Information is available free of charge on the ACS Publications website.

Zeta potentials of the nanocomposites, chronocoulometry characterization of DNA modification, optimization experiments, reproducibility investigation, and DNA/RNA sequences (PDF).

AUTHOR INFORMATION

Corresponding Author

* Tel.: +86-512-69588279. E-mail: miaopeng@sibet.ac.cn (P.M.).

* E-mail: 13812015287@163.com (Y.J.).

Notes

The authors declare no competing financial interest.

ACKNOWLEDGMENT

This work is supported by the National Natural Science Foundation of China (Grant No. 81771929), the Natural Science Foundation of Jiangsu Province for Excellent Young Scholars (Grant No. BK20170087), the Jiangsu Province Young Medical Personnel (Grant No. QNRC2016149), and Wuxi Key Clinical Specialty (Grant No. ZDXK006).

REFERENCES

(1) Lehmann, S. M.; Kruger, C.; Park, B.; Derkow, K.; Rosenberger, K.; Baumgart, J.; Trimbuch, T.; Eom, G.; Hinz, M.; Kaul, D.; Habbel, P.; Kalin, R.; Franzoni, E.; Rybak, A.; Nguyen, D.; Veh, R.; Ninnemann, O.; Peters, O.; Nitsch, R.; Heppner, F. L.; Golenbock, D.; Schott, E.; Ploegh, H. L.; Wulczyn, F. G.; Lehnardt, S. An Unconventional Role for MiRNA: Let-7 Activates Toll-Like Receptor 7 and Causes Neurodegeneration. *Nat. Neurosci.* **2012,** *15*, 827-835.

(2) Li, B.; Fan, J. J.; Chen, N. A Novel Regulator of Type II Diabetes: MicroRNA-143. *Trends Endocrinol. Metab.* **2018,** *29*, 380-388.

(3) Schult, P.; Roth, H.; Adams, R. L.; Mas, C.; Imbert, L.; Orlik, C.; Ruggieri, A.; Pyle, A. M.; Lohmann, V. MicroRNA-122 Amplifies Hepatitis C Virus Translation by Shaping the Structure of the Internal Ribosomal Entry Site. *Nat. Commun.* **2018,** *9*, 2613.

(4) Xing, F.; Liu, Y.; Wu, S. Y.; Wu, K. R.; Sharma, S.; Mo, Y. Y.; Feng, J. M.; Sanders, S.; Jin, G. X.; Singh, R.; Vidi, P. A.; Tyagi, A.; Chan, M. D.; Ruiz, J.; Debinski, W.; Pasche, B. C.; Lo, H. W.; Metheny-Barlow, L. J.; D'Agostino, R. B.; Watabe, K. Loss of XIST in Breast Cancer Activates MSN-c-Met and Reprograms Microglia via Exosomal miRNA to Promote Brain Metastasis. *Cancer Res.* **2018,** *78*, 4316-4330.

(5) Wang, L. L.; Shao, H. H.; Wang, W. J.; Zhang, J. R.; Zhu, J. J. Nitrogen-Doped Hollow Carbon Nanospheres for High-Energy-Density Biofuel Cells and Self-Powered Sensing of MicroRNA-21 and MicroRNA-141. *Nano Energy* **2018,** *44*, 95-102.

(6) Hou, T.; Li, W.; Liu, X. J.; Li, F. Label-Free and Enzyme-Free Homogeneous Electrochemical Biosensing Strategy Based on Hybridization Chain Reaction: A Facile, Sensitive, and Highly Specific MicroRNA Assay. *Anal. Chem.* **2015,** *87*, 11368-11374.

(7) Chen, Z. X.; Peng, Y. J.; Cao, Y.; Wang, H.; Zhang, J. R.; Chen, H. Y.; Zhu, J. J. Light-Driven Nano-oscillators for Label-Free Single-Molecule Monitoring of MicroRNA. *Nano Lett.* **2018,** *18*, 3759-3765.

(8) Islam, M. N.; Masud, M. K.; Haque, M. H.; Hossain, M. S. A.; Yamauchi, Y.; Nguyen, N. T.; Shiddiky, M. J. A. RNA Biomarkers: Diagnostic and Prognostic Potentials and Recent Developments of Electrochemical Biosensors. *Small Methods* **2017,** *1*, 1700131.

(9) Androvic, P.; Valihrach, L.; Elling, J.; Sjoback, R.; Kubista, M. Two-Tailed RT-qPCR: A Novel Method for Highly Accurate MiRNA Quantification. *Nucleic Acids Res.* **2017,** *45*, e144.

(10) Giraldez, M. D.; Spengler, R. M.; Etheridge, A.; Godoy, P. M.; Barczak, A. J.; Srinivasan, S.; De Hoff, P. L.; Tanriverdi, K.; Courtright, A.; Lu, S.; Khoory, J.; Rubio, R.; Baxter, D.; Driedonks, T. A. P.; Buermans, H. P. J.; Nolte-'t Hoen, E. N. M.; Jiang, H.; Wang, K.; Ghiran, I.; Wang, Y. E.; Van Keuren-Jensen, K.; Freedman, J. E.; Woodruff, P. G.; Laurent, L. C.; Erle, D. J.; Galas, D. J.; Tewari, M. Comprehensive Multi-Center Assessment of Small RNA-seq Methods for Quantitative MiRNA Profiling. *Nat. Biotechnol.* **2018,** *36*, 746.

(11) Beaume, M.; Hernandez, D.; Docquier, M.; Delucinge-Vivier, C.; Descombes, P.; Francois, P. Orientation and Expression of Methicillin-Resistant Staphylococcus Aureus Small RNAs by Direct Multiplexed Measurements Using the nCounter of NanoString Technology. *J. Microbiol. Methods* **2011,** *84*, 327-334.

(12) Gai, P. P.; Gu, C. C.; Li, H. Y.; Sun, X. Z.; Li, F. Ultrasensitive Ratiometric Homogeneous Electrochemical MicroRNA Biosensing via Target-Triggered Ru(III) Release and Redox Recycling. *Anal. Chem.* **2017,** *89*, 12293-12298.

(13) Gerasimova, Y. V.; Peck, S.; Kolpashchikov, D. M. Enzyme-Assisted Binary Probe for Sensitive Detection of RNA and DNA. *Chem. Commun.* **2010,** *46*, 8761-8763.

(14) Duan, R. X.; Zuo, X. L.; Wang, S. T.; Quan, X. Y.; Chen, D. L.; Chen, Z. F.; Jiang, L.; Fan, C. H.; Xia, F. Quadratic Isothermal Amplification for the Detection of MicroRNA. *Nat. Protoc.* **2014,** *9*, 597-607.

(15) Ge, L.; Wang, W. X.; Li, F. Electro-Grafted Electrode with Graphene-Oxide-Like DNA Affinity for Ratiometric Homogeneous Electrochemical Biosensing of MicroRNA. *Anal. Chem.* **2017,** *89*, 11560-11567.

(16) Congur, G.; Eksin, E.; Erdem, A. Impedimetric Detection of MicroRNA at Graphene Oxide Modified Sensors. *Electrochim. Acta* **2015,** *172*, 20-27.

(17) Lv, S. F.; Chen, F.; Chen, C. Y.; Chen, X. M.; Gong, H.; Cai, C. Q. A Novel CdTe Quantum Dots Probe Amplified Resonance Light Scattering Signals to Detect MicroRNA-122. *Talanta* **2017,** *165*, 659-663.

(18) Lee, J.; Jin, Y. A.; Ko, H. Y.; Lee, Y. S.; Heo, H.; Cho, S.; Kim, S. Magnetic Resonance Beacon to Detect Intracellular MicroRNA During Neurogenesis. *Biomaterials* **2015,** *41*, 69-78.

(19) Liu, J. T.; Du, P.; Zhang, J.; Shen, H.; Lei, J. P. Sensitive Detection of Intracellular MicroRNA Based on a Flowerlike Vector with Catalytic Hairpin Assembly. *Chem. Commun.* **2018,** *54*, 2550-2553.

(20) Cheng, F. F.; Jiang, N.; Li, X. Y.; Zhang, L.; Hu, L. H.; Chen, X. J.; Jiang, L. P.; Abdel-Halim, E. S.; Zhu, J. J. Target-Triggered Triple Isothermal Cascade Amplification Strategy for Ultrasensitive MicroRNA-21 Detection at Sub-Attomole Level. *Biosens. Bioelectron.* **2016,** *85*, 891-896.

(21) Koo, K. M.; Carrascosa, L. G.; Shiddiky, M. J. A.; Trau, M. Poly(A) Extensions of MiRNAs for Amplification-Free Electrochemical Detection on Screen-Printed Gold Electrodes. *Anal. Chem.* **2016,** *88*, 2000-2005.

(22) Koo, K. M.; Carrascosa, L. G.; Shiddiky, M. J. A.; Trau, M. Amplification-Free Detection of Gene Fusions in Prostate Cancer Urinary Samples Using mRNA-Gold Affinity Interactions. *Anal. Chem.* **2016,** *88*, 6781-6788.

(23) Xu, C.; Pan, C. F.; Liu, Y.; Wang, Z. L. Hybrid Cells for Simultaneously Harvesting Multi-Type Energies for Self-Powered Micro/Nanosystems. *Nano Energy* **2012,** *1*, 259-272.

(24) Miyake, T.; Yoshino, S.; Yamada, T.; Hata, K.; Nishizawa, M. Self-Regulating Enzyme-Nanotube Ensemble Films and Their Application as Flexible Electrodes for Biofuel Cells. *J. Am. Chem. Soc.* **2011,** *133*, 5129-5134.

(25) Zhang, L. L.; Bai, L.; Xu, M.; Han, L.; Dong, S. J. High Performance Ethanol/Air Biofuel Cells with Both the Visible-Light Driven Anode and Cathode. *Nano Energy* **2015,** *11*, 48-55.

(26) Gai, P. P.; Gu, C. C.; Hou, T.; Li, F. Integration of Biofuel Cell-Based Self-Powered Biosensing and Homogeneous Electrochemical Strategy for Ultrasensitive and Easy-To-Use Bioassays of MicroRNA. *ACS Appl. Mater. Interfaces* **2018,** *10*, 9325-9331.

(27) Mishra, P.; Lakshmi, G. B. V. S.; Mishra, S.; Avasthi, D. K.; Swart, H. C.; Turner, A. P. F.; Mishra, Y. K.; Tiwari, A. Electrocatalytic Biofuel Cell Based on Highly Efficient Metal-Polymer Nano-Architectured Bioelectrodes. *Nano Energy* **2017,** *39*, 601-607.

(28) Jiao, K. L.; Kang, Z. P.; Wang, B.; Jiao, S. Q.; Jiang, Y.; Hu, Z. Q. Applying Co3O4@nanoporous Carbon to Nonenzymatic Glucose Biofuel Cell and Biosensor. *Electroanalysis* **2018,** *30*, 525-532.

(29) Zhang, E. H.; Xie, Y.; Ci, S. Q.; Jia, J. C.; Wen, Z. H. Porous Co3O4 Hollow Nanododecahedra for Nonenzymatic Glucose Biosensor and Biofuel Cell. *Biosens. Bioelectron.* **2016,** *81*, 46-53.

(30) Sun, N.; Wen, Z.; Zhao, F. P.; Yang, Y. Q.; Shao, H. Y.; Zhou, C. J.; Shen, Q. Q.; Feng, K.; Peng, M. F.; Li, Y. G.; Sun, X. H. All Flexible Electrospun Papers Based Self-Charging Power System. *Nano Energy* **2017,** *38*, 210-217.

(31) Zhang, Q.; Prabhu, A.; San, A.; Al-Sharab, J. F.; Levon, K. A Polyaniline Based Ultrasensitive Potentiometric Immunosensor for Cardiac Troponin Complex Detection. *Biosens. Bioelectron.* **2015,** *72*, 100-106.

(32) Yu, Y. J.; Zhang, Q.; Buscaglia, J.; Chang, C. C.; Liu, Y.; Yang, Z. H.; Guo, Y. C.; Wang, Y. T.; Levon, K.; Rafailovich, M. Quantitative Real-Time Detection of Carcinoembryonic Antigen (CEA) from Pancreatic Cyst Fluid Using 3-D Surface Molecular Imprinting. *Analyst* **2016,** *141*, 4424-4431.

(33) Guo, Z. Z.; Xu, J.; Zhang, J. Z.; Hu, Y. Y.; Pan, Y.; Miao, P. Facile Strategy for Electrochemical Analysis of Hydrogen Peroxide Based on Multifunctional Fe3O4@Ag Nanocomposites. *ACS Appl. Bio Mater.* **2018,** *1*, 367-373.

(34) Miao, P.; Tang, Y. G.; Mao, Z. Q.; Liu, Y. Z. Adamantane Derivatives Functionalized Gold Nanoparticles for Colorimetric Detection of MiRNA. *Part. Part. Syst. Charact.* **2017,** *34*, 1600405.

(35) Zhen, S. J.; Xiao, X.; Li, C. H.; Huang, C. Z. An Enzyme Free DNA Circuit-Assisted Graphene Oxide Enhanced Fluorescence Anisotropy Assay for MicroRNA Detection with Improved Sensitivity and Selectivity. *Anal. Chem.* **2017,** *89*, 8766-8771.

(36) Zhang, K.; Wang, K.; Zhu, X.; Xu, F.; Xie, M. H. Sensitive Detection of MicroRNA in Complex Biological Samples by Using Two Stages DSN-Assisted Target Recycling Signal Amplification Method. *Biosens. Bioelectron.* **2017,** *87*, 358-364.

(37) Masud, M. K.; Islam, M. N.; Haque, M. H.; Tanaka, S.; Gopalan, V.; Alici, G.; Nguyen, N. T.; Lam, A. K.; Hossain, M. S. A.; Yamauchi, Y.; Shiddiky, M. J. A. Gold-Loaded Nanoporous Superparamagnetic Nanocubes for Catalytic Signal Amplification in Detecting MiRNA. *Chem. Commun.* **2017,** *53*, 8231-8234.

(38) Dai, W. H.; Zhang, J.; Meng, X. D.; He, J.; Zhang, K.; Cao, Y.; Wang, D. D.; Dong, H. F.; Zhang, X. J. Catalytic Hairpin Assembly Gel Assay for Multiple and Sensitive MicroRNA Detection. *Theranostics* **2018,** *8*, 2646-2656.

(39) Feng, C.; Mao, X. X.; Shi, H.; Bo, B.; Chen, X. X.; Chen, T. S.; Zhu, X. L.; Li, G. X. Detection of MicroRNA: A Point-of-Care Testing Method Based on a pH-Responsive and Highly Efficient Isothermal Amplification. *Anal. Chem.* **2017,** *89*, 6631-6636.

(40) Wei, K. J.; Zhao, J. J.; Luo, X. S.; Qiu, S. H.; He, F. Y.; Li, S. T.; Zhao, S. L. An Ultrasensitive Microchip Electrophoresis Assay Based on Separation-Assisted Double Cycling Signal Amplification Strategy for MicroRNA Detection in Cell Lysate. *Analyst* **2018,** *143*, 1468-1474.

(41) Islam, M. N.; Masud, M. K.; Nguyen, N. T.; Gopalan, V.; Alamri, H. R.; Alothman, Z. A.; Al Hossain, M. S.; Yamauchi, Y.; Lam, A. K.; Shiddiky, M. J. A. Gold-Loaded Nanoporous Ferric Oxide Nanocubes for Electrocatalytic Detection of MicroRNA at Attomolar Level. *Biosens. Bioelectron.* **2018,** *101*, 275-281.

(42) Gu, Y.; Song, J.; Li, M. X.; Zhang, T. T.; Zhao, W.; Xu, J. J.; Liu, M. L.; Chen, H. Y. Ultrasensitive MicroRNA Assay via Surface Plasmon Resonance Responses of Au@Ag Nanorods Etching. *Anal. Chem.* **2017,** *89*, 10585-10591.

(43) Hou, T.; Xu, N. N.; Wang, W. X.; Ge, L.; Li, F. Truly Immobilization-Free Diffusivity-Mediated Photoelectrochemical Biosensing Strategy for Facile and Highly Sensitive MicroRNA Assay. *Anal. Chem.* **2018,** *90*, 9591-9597.

(44) Bo, B.; Zhang, T.; Jiang, Y. T.; Cui, H. Y.; Miao, P. Triple Signal Amplification Strategy for Ultrasensitive Determination of miRNA Based on Duplex Specific Nuclease and Bridge DNA-Gold Nanoparticles. *Anal. Chem.* **2018,** *90*, 2395-2400.

(45) Miao, P.; Jiang, Y. T.; Zhang, T.; Huang, Y.; Tang, Y. G. Electrochemical Sensing of Attomolar MiRNA Combining Cascade Strand Displacement Polymerization and Reductant-Mediated Amplification. *Chem. Commun.* **2018,** *54*, 7366-7369.

For Table of Contents Only

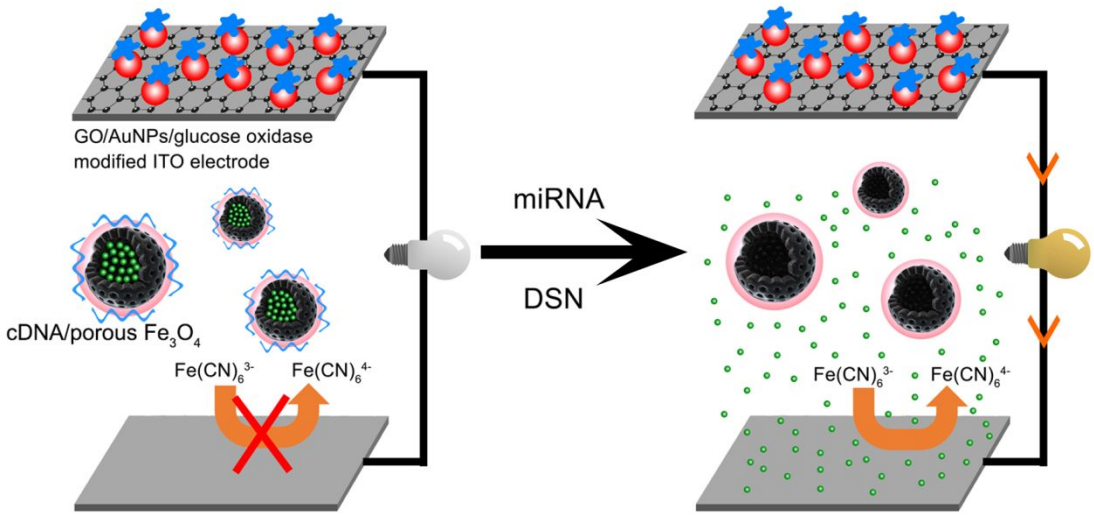

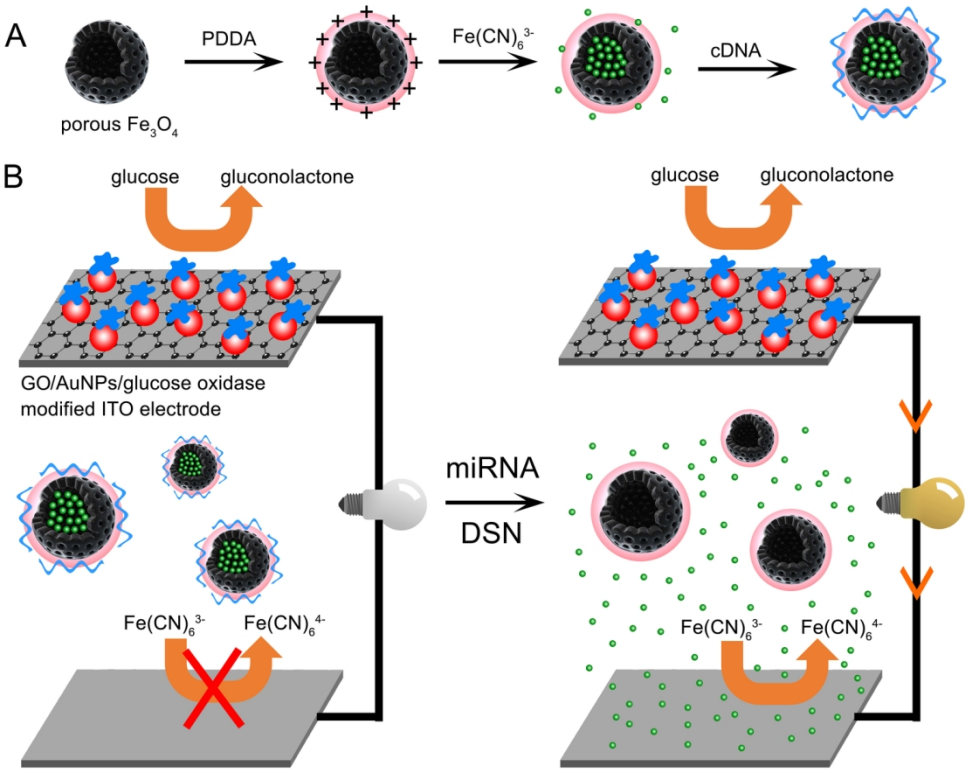

136x109mm (300 x 300 DPI)

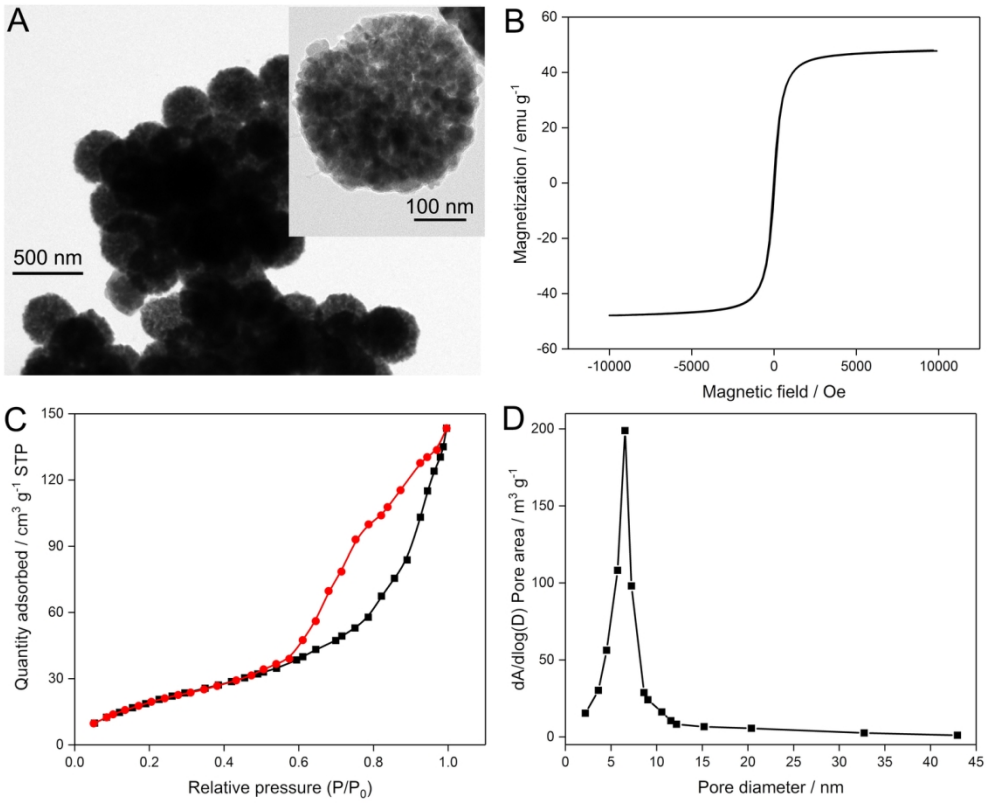

136x110mm (300 x 300 DPI)

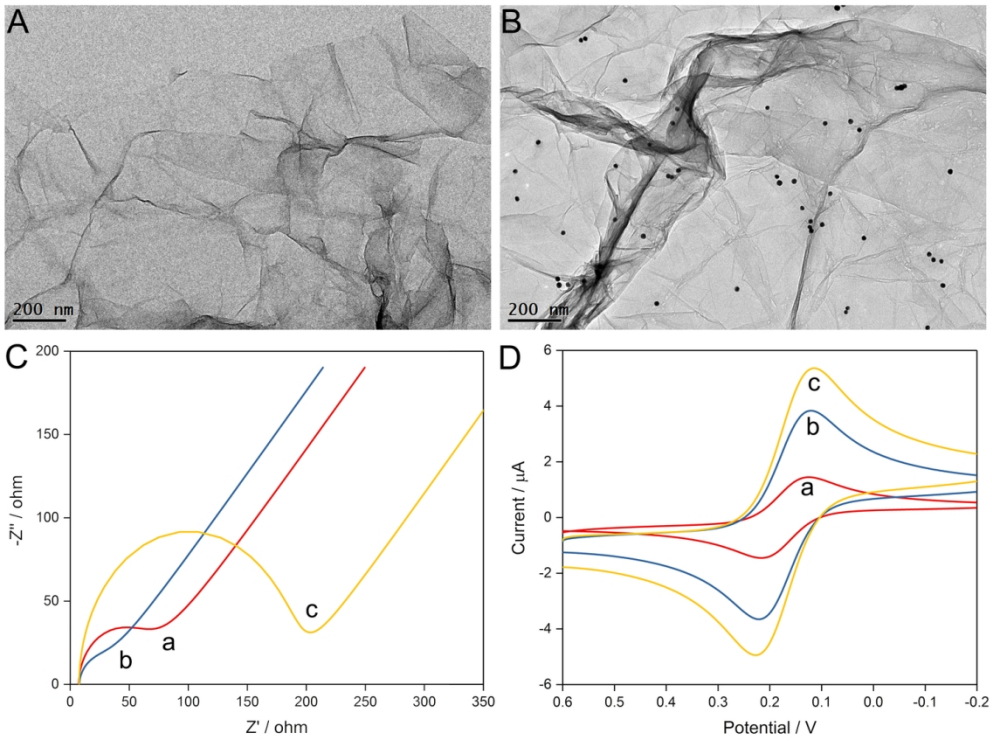

127x95mm (300 x 300 DPI)

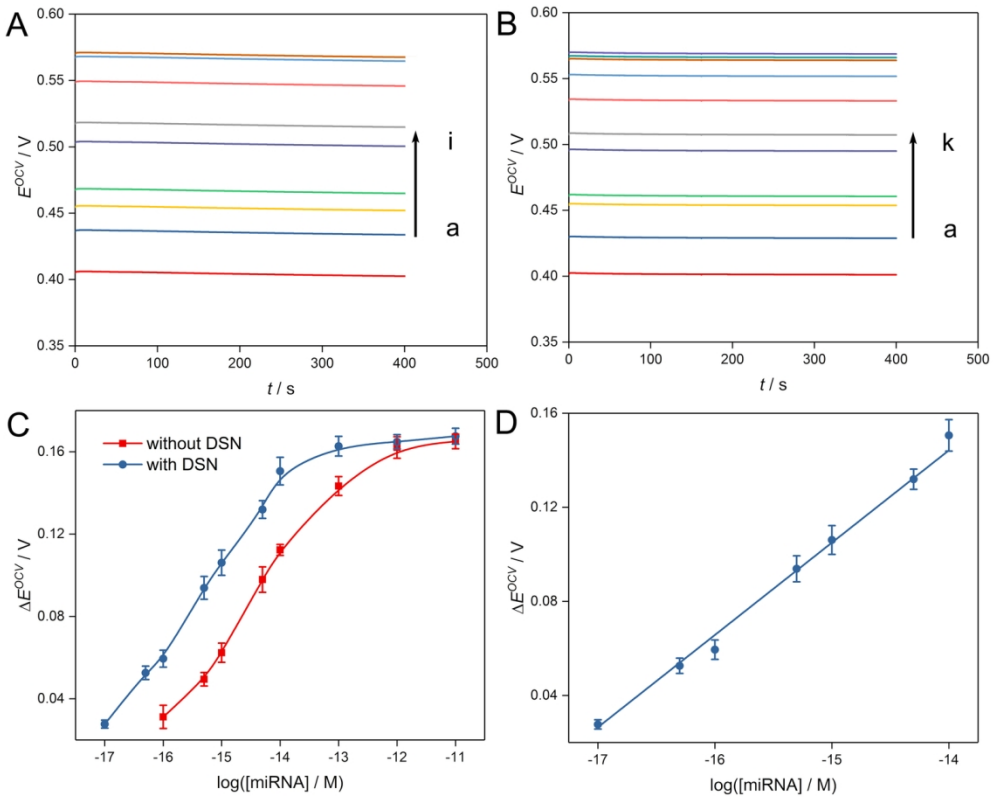

136x110mm (300 x 300 DPI)

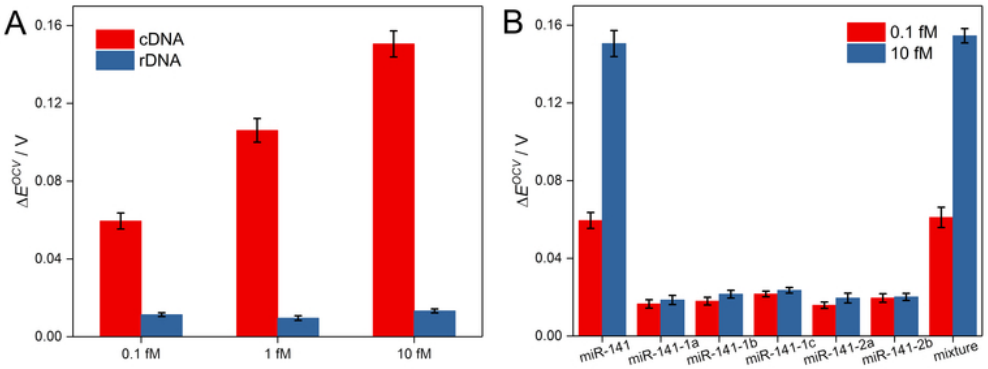

65x24mm (300 x 300 DPI)